Nuclear Medicine and Biology 108–109 (2022) 24–32

Contents lists available at ScienceDirect

Nuclear Medicine and Biology

journal homepage: www.elsevier.com/locate/nucmedbio

Discovery, synthesis and evaluation of novel reversible monoacylglycerol lipase radioligands bearing a morpholine-3-one scaffold

Yingfang He [a], Luca C. Gobbi [b], Adrienne Müller Herde [a], Didier Rombach [b], Martin Ritter [b], Bernd Kuhn [b], Matthias B. Wittwer [b], Dominik Heer [b], Benoit Hornsperger [b], Charles Bell [b], Fionn O'Hara [b], Jörg Benz [b], Michael Honer [b], Claudia Keller [a], Ludovic Collin [b], Hans Richter [b], Roger Schibli [a], Uwe Grether [b], Linjing Mu [a,c,*]

[a] Center for Radiopharmaceutical Sciences, Institute of Pharmaceutical Sciences, Department of Chemistry and Applied Biosciences, ETH Zurich, CH-8093 Zurich, Switzerland
[b] Pharma Research and Early Development, Roche Innovation Center Basel, F. Hoffmann-La Roche Ltd, CH-4070 Basel, Switzerland
[c] Department of Nuclear Medicine, University Hospital Zurich, CH-8091 Zurich, Switzerland

ARTICLE INFO

Article history:
Received 29 November 2021
Received in revised form 29 January 2022
Accepted 14 February 2022

ABSTRACT

Monoacylglycerol lipase (MAGL) is a serine hydrolase that plays an important role in the endocannabinoid degradation in the brain. It has recently emerged as a promising therapeutic target in the treatment of neuroinflammatory and neurodegenerative diseases, such as multiple sclerosis, Alzheimer's disease and Parkinson's disease. Development of MAGL-specific radioligands for non-invasive imaging by positron-emission tomography (PET) would deepen our knowledge on the relevant pathological changes in diseased states and accelerate drug discovery. In this study, we report the selection and synthesis of two morpholine-3-one derivatives as potential reversible MAGL PET tracer candidates based on their multiparameter optimization scores. Both compounds ([^{11}C]**1**, [^{11}C]**2**) were radiolabeled by direct [^{11}C]CO_2 fixation and the *in vitro* autoradiographic studies demonstrated their specificity and selectivity towards MAGL. Dynamic PET imaging using MAGL knockout and wild-type mice confirmed the *in vivo* specificity of [^{11}C]**2**. Our preliminary results indicate that morpholine-3-one derivative [^{11}C]**2** ([^{11}C]**RO7279991**) binds to MAGL *in vivo*, and this molecular scaffold could serve as an alternative lead structure to image MAGL in the central nervous system.

1. Introduction

The endocannabinoid system (ECS) is a lipid-based signaling system involved in numerous physiological processes in the human body [1,2]. *N*-Arachidonoylethanolamine (AEA) and 2-arachidonoylglycerol (2-AG) are the two main and most studied endogenous ligands of the ECS, the so-called endocannabinoids. They are synthesized and released 'on-demand' by neurons in the brain. AEA binds to the cannabinoid 1 and 2 receptors as a partial agonist, while 2-AG acts as a fully effective agonist [3,4]. Fatty acid amine hydrolase (FAAH) and monoacylglycerol lipase (MAGL) are the two primary enzymes that break down AEA and 2-AG, respectively [5]. The hydrolysis of AEA and 2-AG inactivates the endocannabinoid signaling and consequently leads to the production of arachidonic acid (AA). Inhibitors specifically targeting FAAH and MAGL have been investigated for the treatment against a number of diseases, including pain, neurodegenerative disorders, and neuroinflammation [6].

Positron emission tomography (PET) is a non-invasive imaging technique that is capable to visualize and monitor biological processes *in vivo*. In a particular application, PET can be used to assess the target engagement of drug candidates *in vivo*. This supports drug development by providing key data for clinical decision-making, especially for drug candidates targeting proteins in the central nervous system (CNS). A radiolabeled reversible FAAH inhibitor, [^{11}C]MK3168, has been engaged in brain target occupancy studies with single and multiple doses of an orally selective FAAH inhibitor JNJ-4165279 in clinical trials [7]. In contrast, few reversible MAGL PET radiotracers were reported in the last decade [8]. Their chemical structures are shown in Fig. 1, and as highlighted, they generally contain a piperazin-1-yl(thiazol-2-yl) methanone or a 2-(piperazin-1-yl)pyrimidine entity to non-covalently interact with the enzyme in the amphiphilic binding pocket. [^{11}C]PAD and [^{18}F]MAGL-4-11 were substrates of P-glycoprotein (P-gp) expressing at the blood-brain barrier (BBB) and failed to visualize MAGL in rodent brains [9]. [^{18}F]MAGL-2102 was designed based on the structure

* Corresponding author at: Center for Radiopharmaceutical Sciences, Institute of Pharmaceutical Sciences, Department of Chemistry and Applied Biosciences, ETH Zurich, CH-8093 Zurich, Switzerland.
E-mail address: linjing.mu@pharma.ethz.ch (L. Mu).

https://doi.org/10.1016/j.nucmedbio.2022.02.002

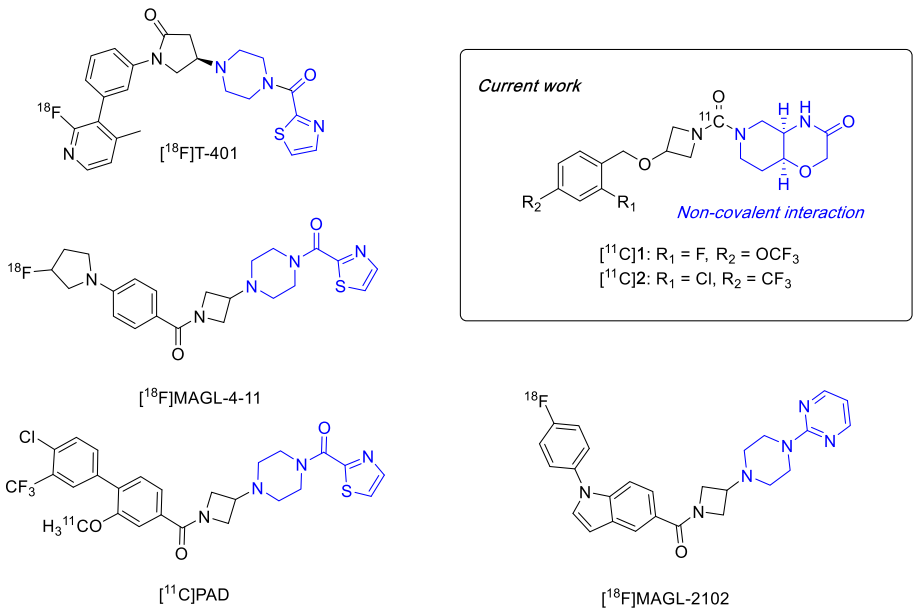

Fig. 1. Chemical structures of reversible MAGL PET radiotracers previously reported and in the current work (Structural entities for non-covalent interaction with MAGL are indicated in blue color).

of [^{18}F]MAGL-4-11 and MAGL drug candidate JNJ-42226314. It displayed sufficient specificity for imaging MAGL in CNS with a slow reversible binding mechanism *in vivo* [10]. Until now, [^{18}F]T-401 stands for the only case as a MAGL PET radiotracer with adequate reversibility within the time frame of PET scans [11].

Recently, we invented a novel series of reversible MAGL inhibitors containing a morpholine-3-one scaffold for the treatment of neuroinflammation [12–14]. The common urea moiety in these molecules facilitates a three-step one-pot carbon-11 radiolabeling approach *via* direct [^{11}C]CO_2 fixation in the presence of phosphazine base [15]. In current work, we sought out to explore the feasibility of this novel structural scaffold as potential reversible MAGL PET radiotracers. To identify the suitable PET tracer candidates from the existing morpholine-3-one library (617 compounds), a set of physiochemical parameters, the so-called multiparameter optimization (MPO) score as previously described was applied for the structural evaluation *in silico* [16]. Two reversible MAGL inhibitors were selected because of their relatively high MPO scores (3.8 and 4.1) and low half maximal inhibitory concentration (IC_{50}) values using human MAGL protein (Fig. 1). Their brain permeabilities were investigated by a passive membrane permeability assay (PAMPA) and by assessing the P-glycoprotein-mediated efflux ratios *in vitro*. In parallel, a lipid membrane binding assay (LIMBA logD) and a plasma protein binding assay were applied to predict their non-specific binding (NSB). The preliminary results using the above-mentioned *in vitro* assays suggested that both compounds should have high brain permeability and low risk of non-specific binding in human. Therefore, compounds **1** and **2** were labeled with carbon-11 by incorporation of [^{11}C]CO_2 with the corresponding amines. Animals or brain tissues from MAGL knockout (KO) and wild-type (WT) mice were enrolled to evaluate their specificity and selectivity in *in vitro* autoradiography and *in vivo* PET studies.

2. Experimental section

2.1. Compound selection

MPO scores were calculated based on the chemical structures in analogy to a previous report [16]. In brief, a monotonic decreasing function was used for the following parameters: lipophilicity (ClogP); machine-learning distribution coefficient (mlLogD at pH = 7.4); molecular weight (M_w); number of hydrogen bond donors (HBD) and the ionization constant value of the most basic center in a substance (pK_a), whereas a hump function was applied to topological polar surface area (TPSA). All the properties were weighted equally with a desirability score ranging from 0.0 to 1.0, and the summation of scores from these parameters yielded the final MPO score of each individual structure. MPO scores of 617 morpholine-3-one derivatives were calculated *in silico* in this study.

2.2. General method

All chemicals, reagents and solvents for the synthesis and analysis of compounds were purchased from commercial sources and used without further purification, unless otherwise specified. (4a*R*,8a*S*)-hexahydro-2*H*-pyrido[4,3-*b*][1,4]oxazin-3(4*H*)-one (HHPO) and 4-nitrophenyl (4a*R*,8a*S*)-3-oxohexahydro-2*H*-pyrido[4,3-*b*][1,4]oxazine-6(5*H*)-carboxylate were synthesized according to the method described previously in the patents [12–14]. All the reactions were monitored by thin-layer chromatography (TLC) performed on Merck TLC glass sheets (silica gel 60 F254), or a Waters Acquity ultra-performance liquid chromatography (UPLC) equipped with a single quadrupole mass spectrometer (MS). Fast column chromatography was carried out using silica gel (Sigma-Aldrich, mesh size 230–400). Nuclear magnetic resonance spectra were acquired on Bruker Avance FT-NMR spectrometer 300, 400 or 600 MHz instruments. Chemical shifts (δ) are reported in parts per million (ppm), relative to the residual solvent peak or trimethylsilane (TMS). High resolution mass spectra were recorded by an Agilent liquid chromatography (LC) system consisting of Agilent 1290 high pressure gradient system, a CTC PAL auto sampler and an Agilent 6520 quadrupole time-of-flight MS. The separation in Agilent LC-system was achieved by Zorbax Eclipse Plus C18 column at 55 °C (1.8 μm 2.1 × 50 mm; phase A = 0.02% formic acid in water, phase B = acetonitrile with 0.01% formic acid at flow 0.8 mL/min; gradient: 0 min 5%B, 0.3 min 5%B, 4.5 min 99%B, 5 min 99%B). The injection volume was 2 μL, and the ionization was performed in Agilent multimode source. The system was run in "2 GHz extended dynamic range" mode, resulting in a resolution of about 10,000 at m/z = 922. Mass accuracy was ensured by internal drift correction.

For the radiosynthesis and quality control after the production, CH_3CN and Milli-Q water containing 0.1% H_3PO_4 were used as phase B

and phase A, respectively. ACE5 C18-300 column (5 μm, 250 × 10 mm) was applied for semi-preparative purification with a gradient method (0.0 min 35%B, 8.0 min 50%B, 12.0 min 60%B, 18.0 min 95%B, 20.0 min 35%B) at a flow rate of 4 mL/min and a wavelength of 254 nM. The quality control was carried out with an Agilent 1100 series HPLC system, equipped with UV detector and a GabiStar radiodetector (Raytest) using an ACE XDB-C18 Zorbax column (3.5 μm, 75 mm × 4.6 mm). The following conditions were used: 0.0 min 35%B, 4.0 min 50%B, 6. 0 min 60%B, 9.0 min 95%B, 10.0 min 35%B at a flow rate of 1 mL/min and a wavelength of 254/230 nM.

2.3. Chemistry

Tert-butyl 3-((2-fluoro-4-(trifluoromethoxy)benzyl)oxy)azetidine-1-carboxylate (**4a**). To a solution of *tert*-butyl 3-hydroxyazetidine-1-carboxylate (200 mg, 1.15 mmol) in anhydrous THF (5 mL) was added potassium *tert*-butoxide (1.65 M solution in THF, 735 μL, 1.21 mmol). The reaction mixture was stirred at room temperature for 15 min, followed by addition of **3a** (315 mg, 1.15 mmol) in THF, and stirring at room temperature for 14 h. The reaction was then diluted with ethyl acetate and extracted with aq. 1 M $NaHCO_3$. The organic phase was collected and the aqueous phase was back-extracted with ethyl acetate. The combined organic phases were dried over Na_2SO_4, and evaporated down to dryness. The crude product (418 mg) was used in the next step without further purification. ^{1}H NMR (300 MHz, Chloroform-*d*) δ 7.45 (t, *J* = 8.3 Hz, 1H), 7.09–7.01 (m, 1H), 7.00–6.92 (m, 1H), 4.49 (s, 2H), 4.39–4.29 (m, 1H), 4.12–4.06 (m, 2H), 3.90–3.82 (m, 2H), 1.44 (s, 9H). LC-MS (ESI): *m/z* = 310.1 $[M-56+H]^+$.

3-((2-Fluoro-4-(trifluoromethoxy)benzyl)oxy)azetidine 2,2,2-trifluoroacetate (**5a**). To a solution of **4a** (415 mg, 1.14 mmol) in DCM (5 mL), TFA (875 μL, 11.4 mmol) was added. The reaction mixture was stirred at room temperature for 3 h. The solvent was removed to yield 455 mg of a light-yellow oil, which was used in the next step without any further purification. ^{1}H NMR (300 MHz, DMSO-d_6) δ 7.63 (t, *J* = 8. 4 Hz, 1H), 7.49–7.39 (m, 1H), 7.35–7.21 (m, 1H), 4.56 (s, 2H), 4.52–4. 40 (m, 1H), 4.28–4.06 (m, 2H), 3.99–3.74 (m, 2H). LC-MS (ESI): *m/z* = 266.1 $[M+H]^+$. For radiosynthesis, the crude product was further purified by Merck-Hitachi LaChrom HPLC system using semi-preparative reverse-phase C18 column (5 μm, 10 × 150 mm, Sunfire™, Waters, USA). The mobile phase consists of 0.1% TFA in Milli-Q water and acetonitrile for phase A and B, respectively. A gradient method with 0–15 min, 10–50%B; 15–17 min, 50–90%B; 17–20 min, 90–10%B was used, and the flow was set to 4 mL/min. Under the wavelength of 254 nm, the product was collected and its identity was confirmed by LC-MS. The collected fraction was lyophilized to obtain the entitled compound as a white solid qualified for radiolabeling.

(4a*R*,8a*S*)-6-(3-((2-Fluoro-4-(trifluoromethoxy)benzyl)oxy) azetidine-1-carbonyl)hexahydro-2*H*-pyrido[4,3-*b*][1,4]oxazin-3(4*H*)-one (**1**). To a solution of 4-nitrophenyl (4a*R*,8a*S*)-3-oxohexahydro-2*H*-pyrido[4,3-*b*][1,4]oxazine-6(5*H*)-carboxylate (50 mg, 156 μmol) in CH_3CN (1 mL) was added DIPEA (60.3 mg, 81.5 μL, 467 μmol) and **5a** (67.9 mg, 179 μmol). The reaction mixture was then stirred at 90 °C for 4 h. The solvent was removed under reduced pressure and the crude residue was purified by reverse-phase HPLC to yield the desired product as a white powder (45 mg, 65%). ^{1}H NMR (600 MHz, Chloroform-*d*) δ 7.44 (t, *J* = 8.3 Hz, 1H), 7.04 (dt, *J* = 8.5, 1.1Hz, 1H), 6.97 (dd, *J* = 10.1, 1.4 Hz, 1H), 6.47 (br d, *J* = 3.9 Hz, 1 H, —NHCO—), 4.49 (s, 2H), 4.34–4.37 (m, 1H), 4.26–4.31 (m, 1H), 4.17–4.22 (m, 1H), 4.16–4.22 (m, 1H), 4.10–4.15 (m, 1H), 3.94–3.99 (m, 1H), 3.92–3.98 (m, 1H), 3.86–3.92 (m, 2H), 3.48 (ddt, *J* = 13.5, 5.0, 1.9, 1.9 Hz, 1H), 3. 33–3.43 (m, 1H), 3.00–3.12 (m, 2H), 1.87–1.97 (m, 1H), 1.79 (dddd, *J* = 14.5, 12.8, 5.2, 3.2 Hz, 1H). ^{13}C NMR (150 MHz, Chloroform-*d*): δ 168.4, 162.1, 160.5, 149.5, 131.0, 123.1, 120.3, 116.7, 108.9, 69.4, 68.1, 67.6, 63.8, 58.4, 58.2, 49.5, 46.2, 39.8, 29.5. HR-MS: *m/z* 448.1492; calc. for $C_{19}H_{21}F_4N_3O_5 + H^+$ 448.1490.

Tert-butyl 3-((2-chloro-4-(trifluoromethyl)benzyl)oxy)azetidine-1-carboxylate (**4b**). The procedure described for the synthesis of **4a** was applied to *tert*-butyl 3-hydroxyazetidine-1-carboxylate (200 mg, 1.15 mmol), potassium *tert*-butoxide (1.65 M solution in THF, 735 μL, 1.21 mmol) and **3b** (316 mg, 1.15 mmol) to obtain the crude product (429 mg). ^{1}H NMR (300 MHz, Chloroform-*d*) δ 7.70–7.49 (m, 3H), 4.57 (s, 2H), 4.45–4.33 (m, 1H), 4.16–4.06 (m, 2H), 4.02–3.86 (m, 2H), 1.45 (s, 9H). LC-MS (ESI): *m/z* = 310.1 $[M-56+H]^+$.

3-((2-Chloro-4-(trifluoromethyl)benzyl)oxy)azetidine 2,2,2-trifluoroacetate (**5b**). The experimental procedure described for synthesis of **5a** was applied to synthesize **5b** by reacting **4b** (426 mg, 1.16 mmol) with TFA (718 μL, 9.32 mmol) to yield the crude product (457 mg). It can be used in the next step without further purification expect in the case for radiolabeling, which was further purified by semi-preparative HPLC as described for **5a**. ^{1}H NMR (400 MHz, Chloroform-*d*) δ 7.66–7.63 (m, 1H), 7.61–7.54 (m, 2H), 4.60 (s, 2H), 4.59–4.52 (m, 1H), 4.26–4.18 (m, 2H), 4.14–3.99 (m, 2H). LC-MS (ESI): *m/z* = 266.1 $[M+H]^+$.

(4a*R*,8a*S*)-6-(3-((2-Chloro-4-(trifluoromethyl)benzyl)oxy) azetidine-1-carbonyl)hexahydro-2*H*-pyrido[4,3-b][1,4]oxazin-3(4*H*)-one (**2**). The procedure described for the synthesis of **1** was applied to 4-nitrophenyl (4a*R*,8a*S*)-3-oxohexahydro-2*H*-pyrido[4,3-b][1,4]oxazine-6(5*H*)-carboxylate (50 mg, 156 μmol), DIPEA (60.3 mg, 81.5 μL, 467 μmol) and **5b** (88.6 mg, 233 μmol) to yield the desired product as white powder (34 mg, 49%). ^{1}H NMR (600 MHz, Chloroform-*d*) δ 7.63 (s, 1H), 7.64 (s, 1H), 7.55 (dd, *J* = 7.7, 1.5 Hz, 1H), 6.13 (br d, *J* = 3.8 Hz, 1H, —NHCO—), 4.58 (s, 2H), 4.41 (tt, *J* = 6.5, 4.3 Hz, 1H), 4.28–4. 33 (m, 1H), 4.23–4.26 (m, 1H), 4.17–4.23 (m, 1H), 4.17–4.22 (m, 1H), 4.14–4.17 (m, 1H), 4.02 (td, *J* = 4.6, 0.9 Hz, 1H), 3.98 (q, *J* = 2.8 Hz, 1H), 3.90 (dd, *J* = 13.0, 4.9 Hz, 1H), 3.50 (ddt, *J* = 13.5, 5.1, 2.0, 2.0 Hz, 1H), 3.37–3.44 (m, 1H), 3.01–3.15 (m, 2H), 1.93 (dq, *J* = 14.4, 2.7 Hz, 1H), 1.80 (dddd, *J* = 14.5, 12.8, 5.3, 3.2 Hz, 1H). ^{13}C NMR (150 MHz, Chloroform-*d*) δ 168.2, 162.2, 139.2, 132.9, 131.4, 129.0, 126.3, 123.8, 123.8, 69.4, 68.5, 67.7, 67.3, 58.4, 58.2, 49.6, 46.2, 39.8, 29.5. HR-MS: *m/z* 448.1251; calc. for $C_{19}H_{21}ClF_3N_3O_4 + H^+$ 448.1245.

2.4. Radiosyntheses of [^{11}C]**1** and [^{11}C]**2**

A direct $^{11}CO_2$ fixation method previously reported was modified and employed for radiolabeling [15]. Briefly, [^{11}C]CO_2 produced *via* ^{14}N (p, α) ^{11}C nuclear reaction in a cyclone 18/9 cyclotron (18-MeV; IBA, Ottignies-Louvain-la-Neuve, Belgium) and was trapped in a stainless steel loop using liquid nitrogen. Upon warming, the [^{11}C]CO_2 gas together with a stream of argon gas was first passed through a P_2O_5 column, then slowly bubbled into a mixture of HHPO (0.672 mg, 4.3 μmol) and 2-*tert*-butylimino-2-diethylamino-1,3-dimethylperhydro-1, 3,2-diazaphosphorine (BEMP, 5 μL, 17.3 μmol) in 100 μL anhydrous DMF. The reaction was kept at ambient temperature for 2 min and stirred gently by a mild helium flow. Afterwards, 0.2% $POCl_3$ (v/v) in MeCN (100 μL, 2.15 μmol) was added into the mixture and reacted for 1 min. The corresponding azetidine (4.7 μmol in 100 μL MeCN) was then added and the reaction mixture was reacted for further 2 min at ambient temperature. The reaction mixture was subsequently diluted with 2 mL H_2O and injected into a semi-preparative HPLC column for purification. The desired product was collected within a retention time between 9 and 11 min, diluted with 8 mL H_2O, and passed through a light Sep-Pak C18 cartridge (Waters). After washing with 5 mL water, the radioligand was eluted with 0.5 mL EtOH. The formulated solution containing 5% ethanol was obtained by adding 9.5 mL 0.15 M phosphorus buffer (pH = 7.4), and used for all *in vitro*/*in vivo* studies.

2.5. MAGL IC_{50} measurement and in vitro characterizations

2.5.1. MAGL IC_{50} measurement

The IC_{50} values of compounds **1** and **2** were measured using human or mouse MAGL. Briefly, the compound was prepared in concentrations

ranging from 70 pM to 12.5 μM. The dilutions were transferred into a 384-well plate containing recombinant MAGL protein in assay buffer (50 mM TRIS, 1 mM EDTA, 0.01% Tween 20, v/v and 2.3% DMSO, v/v). After incubating at room temperature for 15 min, 2-AG in assay buffer was added to initialize the hydrolysis. The final concentration of MAGL protein was 50 pM, and 8 μM for 2-AG and 2.5% (v/v) for DMSO. The plate was incubated at room temperature with gentle shaking for further 30 min, followed by the addition of a double assay volume of acetonitrile containing 4 μM d_8-AA to quench the reaction. The hydrolytic rate of the enzyme was monitored by an online solid phase extraction (SPE) system (Agilent Rapidfire) coupled to a triple quadrupole mass spectrometry (Sciex5000 or Agilent 6460) in ESI^- mode, and determined by the intensity of AA (m/z = 303.1 to 259.1) to d_8-AA (m/z = 311.1 to 267.1). The IC_{50} values were obtained after fitting the intensity ratio of the AA/d_8-AA under various concentrations into saturation equation. The IC_{50} values from individual measurement are provided in the supporting information.

2.5.2. Determination of drug binding to plasma proteins

The free fractions of the compound in human and mouse plasma were determined by equilibrium dialysis as previously described [17]. A detailed procedure is given in the supporting information.

2.5.3. P-glycoprotein-mediated efflux ratios

The experimental procedure for *in vitro* transport studies with compounds **1** and **2** was described as previously reported [18,19]. Porcine kidney epithelial LLC-PK1 cells stably transfected with Abcb1a (Mdr1a, mouse P-gp) or ABCB1 (Mdr1, human P-gp) were provided by Dr. A. Schinkel (Netherlands Cancer Institute). The cells were cultured with Medium 199 Glutamax (Gibco/Life Technologies) supplemented with 10% fetal bovine serum, 1% penicillin/streptomycin (Amimed, Basel, CH) and 100 ng/mL colchicine (SERVA Electrophoresis Gmbh, Heidelberg, DE) at 37 °C in a humidified 5% CO_2 incubator, and seeded at a density of 1.4×10^5 cells/well on porous poly (ethylene terephthalate) membrane filters 4 days prior to the experiment. On the experimental day, the culture medium was removed from barrier between apical (A) and basolateral (B) compartments and replaced with medium without phenol red. The measurement of transcellular transport was triggered by the addition of 1 μM compound **1** or **2** to the donor side, corresponding to a total volume of 100 μL on the apical side or 240 μL on the basolateral side, and carried out in both apical-to-basolateral (A → B) and basolateral-to-apical (B → A) directions in triplicates. The resulting inserts were incubated at 37 °C and 5% CO_2 for 3 h. Samples (20 μL) were taken from both donor and receiver sides at the end of the incubation, and the concentration of the test compound was determined by high performance liquid chromatography–tandem mass spectrometry. The apparent permeability (P_{app}) in the basolateral-to-apical direction ($P_{app}^{B\rightarrow A}$) and apical-to-basolateral direction ($P_{app}^{A\rightarrow B}$) were calculated. The efflux ratios of the compounds were determined as the ratio of $P_{app}^{B\rightarrow A}$ to $P_{app}^{A\rightarrow B}$. The cell lines were passaged at least three times before the experiments. To ensure Mdr1a functionality, the efflux ratio of ^{3}H-digoxin, a typical Mdr1a substrate, was measured in each incubation plate as a control using scintillation counting. Additionally, the tightness of the cell monolayer was controlled by extracellular marker (Lucifer yellow, Sigma-Aldrich, St. Louis, MO) and quantified using Spectra Fluor Plus Reader at 430/535 nm excitation/emission.

2.5.4. Passive membrane permeability assay (PAMPA)

The PAMPA assay was carried out as a high throughput experiment in 96-deepwell plate (Thermo Fisher Scientific, Waltham, MA; volume well: 2200 μL). The compound was dissolved in DMSO in a concentration of 10 mM. The drug solution (15 μL) was added into the plate containing donor buffer (985 μL, 50 mM 3-morpholino-2-hydroxypropanesulfonic acid with 0.5% glycocholic acid, pH = 6.0) in each well. The mixture was later filtered through a filter plate coated with a phospholipid-containing solution (ø 0.45 μm, MultiScreen Deep Well Solvinert, Merck Millipore, Darmstadt, Germany), and analyzed using a Spectramax plus 384 UV reader (Molecular Devices, Sunnyvale, CA) in the wavelength of 246–650 nm as previously reported to determine the permeability [17].

2.5.5. Lipid membrane binding assay

Lipid membrane binding assay (LIMBA logD) was performed analogous to previous reports as high/medium throughput measurements [17,20,21]. A detailed procedure is given in the supporting information.

2.5.6. Lipophilicity and in vitro stability

[^{11}C]**1** or [^{11}C]**2** (10 μL, 5–10 MBq) was pipetted into an Eppendorf tube containing 500 μL of *n*-octanol and 500 μL of phosphate buffer (0.02 M, pH = 7.4). The tube was shaken for 15 min at room temperature, and the two phases were separated by centrifugation at 5000 rpm for 3 min. 50 μL Sample from the *n*-octanol layer was pipetted in a vial and measured on an automatic γ-counter (Wizard; PerkinElmer), as well as 50 μL sample from the buffer layer. 100 μL sample from organic layer was taken into another Eppendorf tube with *n*-octanol (400 μL) and sodium phosphate buffer (500 μL) inside for further redistribution until distribution coefficient values were consistent. The partition coefficient was calculated using Eq. (1).

$$\log D_{7.4} = \log \frac{\text{counts per minute (octanol)}}{\text{counts per minute (phosphate buffer)}} \quad (1)$$

To test the *in vitro* stability, the radioligand was incubated with mouse or human serum at 37 °C. After 40 min incubation, the mixture of serum was treated with equal amount of ice-cold acetonitrile to precipitate extra protein. The sample was then centrifuged at 14000 rpm for 5 min, passed through a 0.22 μM Nalgene PES syringe filter (Thermo Scientific, Waltham, MA) and analyzed by radio-ultra-performance liquid chromatography (UPLC). Furthermore, the formulated solution was analyzed by UPLC after 1 h storage at room temperature to evaluate the stability of the radioligand.

2.5.7. In vitro autoradiography

Brain tissues from Wistar rats or C57/Bl6 mice were prepared as sections of 10 μm thickness using a cryostat (Cryo-Star HM 560 MV; Microm, Thermo Scientific, Wilmington, DE), and stored at −20 °C. Shortly before the experiment, the sections were taken out from the freezer, thawed on ice, and preconditioned in an aqueous buffer comprising 30 mM HEPES, 1.2 mM $MgCl_2$, 110 mM NaCl, 5 mM KCl, 2.5 mM $CaCl_2$, and 0.1% fatty acid free bovine serum albumin (pH 7.4, 0 °C) for 10 min. After drying in the air, incubation was carried out with 8–12 nM of radioligand in a humidified chamber for 30 min. For blocking experiments on Wistar brain sections, radioligand with 10 μM SAR127303 or 10 μM PF-06795071 was applied for incubation. Upon the completion, the slices were subsequently washed in the incubation buffer mentioned above (pH 7.4, 0 °C, 1 × 2 min) and washing buffer consisting of 30 mM HEPES, 1.2 mM $MgCl_2$, 110 mM NaCl, 5 mM KCl, 2.5 mM $CaCl_2$ (pH 7.4, 0 °C, 2 × 2 min). Following by 2 quick dips in distilled water, the sections were dried at room temperature before exposure to a phosphor imager plate (Fuji, Dielsdorf, Switzerland) for 60–90 min. The films were scanned by a BAS5000 reader (Fuji), and AIDA 4.50.010 software (Raytest Isotopenmessgeräte GmbH, Straubenhardt, Germany) was used for data analysis.

For no-wash *in vitro* autoradiography, the incubation time was shortened to 20 min as previously reported [22]. The slides were rapidly dipped in distilled water (< 3 s) to remove adhering droplets from the incubation buffer, and left to dry at room temperature before exposure. Semi-quantification of radioactive signals in *in vitro* autoradiography was carried out using AIDA 4.50.010 software (Raytest Isotopenmessgeräte GmbH, Straubenhardt, Germany) based on the

density of photostimulated luminescence (PSL) in the whole brain area (pixel) expressed PSL per pixel. The percentage of specific binding was calculated using Eq. (2). Corresponding results under control and blocking conditions were statistically evaluated with Student's *t*-test (two-tailed, homoscedastic) using Microsoft Excel 2013.

$$\%\text{Specific binding}_{20\ \text{min}} = \frac{\textit{Density in baseline} - \textit{Density in blockade}}{\textit{Density in baseline}} \times 100\% \quad (2)$$

2.6. In vivo characterizations

MAGL KO mice (strain name: HLR0027_Mgll KO, 2 males and 1 female, 12–14 weeks old, body weight: 20.3–32.5 g) and the age- and gender- matched C57BL/6NTac mice were purchased from Taconic. The animals were housed in groups accounting for gender under standard conditions (12:12 h light-dark cycle, free access to food and water). The healthy C57BL/6 mice for radiometabolite analysis and P-gp inhibition was supplied by Charles River Laboratories (Sulzfeld, Germany). All animals were taken care in compliance with the Swiss Animal Welfare Legislation, and the experiments were authorized by the Veterinary Office of the Canton Zurich (Reference number: ZH28/2018).

2.6.1. Dynamic PET scans

Isoflurane was used for anesthesia, and the animal was immobilized inside a Super Argus PET/CT tomography (Sedecal, Madrid, Spain). Dynamic PET scans started 1 min after the injection of [^{11}C]**2** (10.04–14.30 MBq) *via* the tail vein to the animal. The respiratory frequency of the animal was tracked by an external monitor (SA Instruments, Inc., Stony Brook), and CT scanning was acquired immediately after 60 min PET scanning. The collected data was reconstructed under user-defined time frames with a voxel size of 0.3875 × 0.3875 × 0.775 mm^3, and the images were analyzed with PMOD 4.002 software (PMOD Technologies Ltd., Zurich, Switzerland). A MRI T2 P × Mouse (W. Schiffer) template provided by PMOD was used to define the regions of interest (ROIs). The radioactive accumulation was given as standardized uptake value (SUV), which is the decay-corrected image-derived radioactivity per cm^3 tissue (multiplied with 1 g/cm^3), divided by the injected radioactivity dose per gram of body weight [23]. Detailed information on MAGL KO and WT mice and the PET study plans is provided in supporting information Table S1. For P-gp inhibition study, tariquidar was prepared as reported in the literatures [24,25] and the mouse was treated with 7.5 mg/kg tariquidar at 45 min pre-injection.

2.6.2. Radiometabolite analysis

Ex vivo radiometabolite analysis was performed using healthy C57BL/6 mouse (n = 1). [^{11}C]**2** was administrated intravenously *via* tail vein, and the animal was scarified by decapitation at 40 min post-injection. The blood was collected immediately in a heparin-coated tube, and transferred to an Eppendorf tube with ice-cold acetonitrile. After vortexing and centrifugation at 5000 *g* for 5 min, the supernatant was passed through a 0.22 μM Nalgene PES syringe filter (Thermo Scientific, Waltham, MA) as the plasma sample. Similar procedure was applied to the preparation of the urine sample. For the brain sample, homogenate was firstly obtained in 1 mL PBS buffer after dissection. The mixture was centrifuged at 5000 *g* for 5 min with additional 1 mL ice-cold acetonitrile. The supernatant was passed through a 0.22 μM Nalgene PES syringe filter and prepared as the brain sample. Radio-UPLC equipped with BEH C18 column (Acquity Waters, 130 Å, 1.7 μm, 2.1 mm × 50 mm) was used to analyze the samples (mobile phase A: 10 mM NH_4HCO_3 in Milli-Q water, mobile phase B: acetonitrile; 0.0–2.0 min, 5–30%B; 2.0–3.5 min, 30–50%B; 3.5–4.0 min, 50–90%B; 4.0–6.0 min, 90%B at a flow rate of 0.6 mL/min and a wavelength of 254 nm).

3. Results

3.1. Chemistry

The syntheses of compounds **1** and **2** are illustrated in scheme 1. Briefly, compounds **4a** and **4b** were prepared *via O*-alkylation of *tert*-butyl 3-hydroxyazetidine-1-carboxylate with benzyl bromides **3a** and **3b,** respectively. After removing the *tert*-butyloxycarbonyl group with trifluoroacetic acid, the corresponding azetidines **5a** and **5b** were obtained as trifluoroacetate salts. In the last step, azetidines **5a** and **5b** were reacted with nitrophenol activated hexahydro-2*H*-pyrido-oxazin-one carboxylate to form the desired urea compounds **1** and **2** in 65% and 49% yield, respectively.

3.2. Radiosyntheses of [^{11}C]**1** and [^{11}C]**2**

Following the steps presented in scheme 2, carbon-11 was incorporated into the unsymmetrical urea structure *via* a three-step, one-pot reaction. Firstly, [^{11}C]CO_2 was trapped in a solution of 2-*tert*-butylimino-2-diethylamino-1,3-dimethylperhydro-1,3,2-diazaphosphorine (BEMP) and (4a*R*,8a*S*)-hexahydro-2*H*-pyrido[4,3-*b*][1,4]oxazin-3(4*H*)-one (HHPO) in anhydrous DMF (100 μL). A carbamoyl chloride was presumably formed with sequential addition of phosphoryl trichloride ($POCl_3$) in 100 μL of acetonitrile, which further reacted with azetidine **5a** or **5b** to yield the desired asymmetric carbon-11 labeled urea [^{11}C]

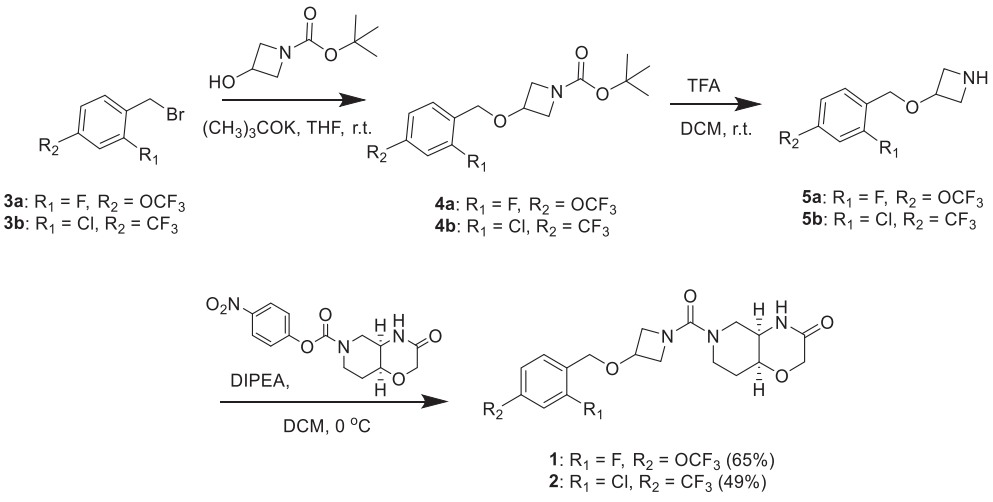

Scheme 1. Syntheses of compounds **1** and **2**.

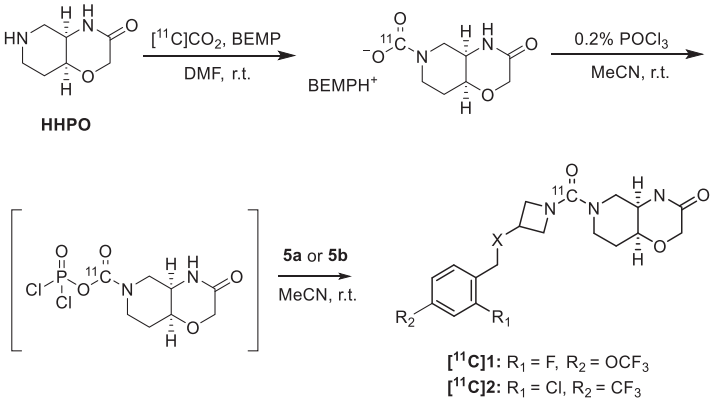

Radiotracer	RCY (%)	n
[^{11}C]**1**	1.4 ± 0.2	3
[^{11}C]**2**	1.3 ± 0.3	8

Scheme 2. Radiosyntheses of [^{11}C]**1** and [^{11}C]**2**. The RCYs over three steps were non-decay corrected and calculated upon the estimated amount of [^{11}C]CO_2 trapped in the reaction vial.

1 or [^{11}C]**2**. Upon quenching the reaction, the reaction mixture was loaded into a semi-preparative HPLC column for purification. This three-step, one-pot synthesis gave [^{11}C]**1** (0.85–1.17 GBq, n = 3) and [^{11}C]**2** (0.82–1.10 GBq, n = 8) with high radiochemical purity greater than 99%. The molar activities at the end of synthesis were 95 ± 22 GBq/μmol (n = 3) for [^{11}C]**1** and 82 ± 34 GBq/μmol (n = 8) for [^{11}C]**2**. The total synthesis time was around 30 min from the end of bombardment.

3.3. In vitro characterizations

3.3.1. IC_{50} measurement and pharmacological properties

Table 1 summarizes the IC_{50} values of compounds **1** and **2** towards MAGL and their pharmacological properties. The IC_{50} values were determined using mouse and human MAGL enzymes, respectively. Both compounds displayed potent MAGL inhibition at low nanomolar concentrations. Compound **2** demonstrated slightly higher potency towards human and mouse MAGL than compound **1**. Free fraction (f_P) of compound **1** is two-fold higher than that of compound **2** in either human or mouse plasma. LIMBA logD values are 1.0 and 1.3 for compounds **1** and **2**, respectively, predicting a low degree of non-specific binding in human brain [20]. High P-gp efflux ratios (≥6.9) in mice and low P-gp ratios (~2.1) in human indicated that these compounds are more likely to be recognized as P-gp substrates in rodents rather than in human. Additionally, compounds **1** and **2** possess sufficient passive membrane permeability ($P_{eff} > 2 \times 10^{-6}$ cm/s) [17] as well as desirable physiochemical properties (CNS MPO score > 3), suggesting a high brain penetration in human.

3.3.2. Lipophilicity and in vitro stability

The partition coefficient log$D_{7.4}$ of the ^{11}C-labeled radioligands was determined by the shake-flask method as previously described [26]. [^{11}C]**1** containing trifluoromethoxyl and fluorine substituents in the aromatic ring showed lower lipophilicity with a log $D_{7.4}$ value of 1.58 ± 0.04 compared to [^{11}C]**2** (log $D_{7.4}$ = 2.21 ± 0.03, n = 3). This observation is in agreement with the lower LIMBA log *D* and higher free fraction of compound **1** in previous investigations. In *in vitro* stability evaluation, both radiotracers remained above 95% purity after 40 min incubation with mouse or human serum at 37 °C. Furthermore, [^{11}C]**1** and [^{11}C]**2** were stable in the final formulation after 1 h storage at room temperature (RCP > 99%).

3.3.3. In vitro autoradiography

To investigate the *in vitro* specificities of the radiotracers, autoradiographic studies were performed using sagittal brain sections from Wistar rats. Both radiotracers revealed a heterogeneous distribution in line with MAGL expression patterns in rat brain: high levels of accumulation were observed in the cortex, striatum, hippocampus and thalamus, while moderate radioactive accumulation was found in the cerebellum (Fig. 2A) [27]. Co-incubation with an irreversible MAGL inhibitor, either 10 μM SAR127303 or PF-06795071, led to significant reduction of the radioactive signals in the MAGL-rich brain regions indicating the specificity of the radioligands *in vitro*. Brain sections from MAGL KO and the corresponding WT mice were further included to investigate the off-target binding. Similar to the previous results using Wistar rat brain sections under blocking conditions, homogenous and low radioactive signals were obtained on MAGL KO brain slices. These results confirmed the selectivity and specificity of [^{11}C]**1** and [^{11}C]**2** towards MAGL in rodents *in vitro*.

Moreover, *in vitro* autoradiography was performed on Wistar brain sections using [^{11}C]**2** without washing procedures to mimic the *in vivo* situation [22]. The brain slices were dipped in distilled water quickly after short incubation, and autoradiograms from no-wash procedure are presented in Fig. 2B. In the absence of the washing procedure, [^{11}C]**2** produced specific signals with heterogeneous distribution after 20 min incubation on rat brain tissues. In the presence of excessive amount of covalent MAGL inhibitor (10 μM SAR127303 or 10 μM PF-0679507), similar blocking effect was observed in comparison with autoradiograms processed including the normal washing procedure. Semi-quantification revealed that the specific binding of [^{11}C]**2** was 39% with 10 μM SAR127303, and 44% with 10 μM PF-06795071 as the blocker, respectively (Table 2). A significant difference regarding the radioactive densities was obtained between the control and blocking groups ($p < 0.001$).

3.4. In vivo characterization

3.4.1. Dynamic PET scan

Table 1
In vitro characterizations of compounds **1** and **2**.

Compd	Mouse			Human			LIMBA logD	PAMPA P_{eff} [cm/s·10^{-6}]	CNS MPO score
	IC_{50} (nM, n = 3)	f_P (%)	P-gp ER	IC_{50} (nM, n = 3)	f_P (%)	P-gp ER			
1	34 ± 5	24	7.5	12 ± 1	22	2.1	1.0	4.3	3.8
2	19 ± 7	11	6.9	5 ± 2	11	2.1	1.3	3.9	4.1

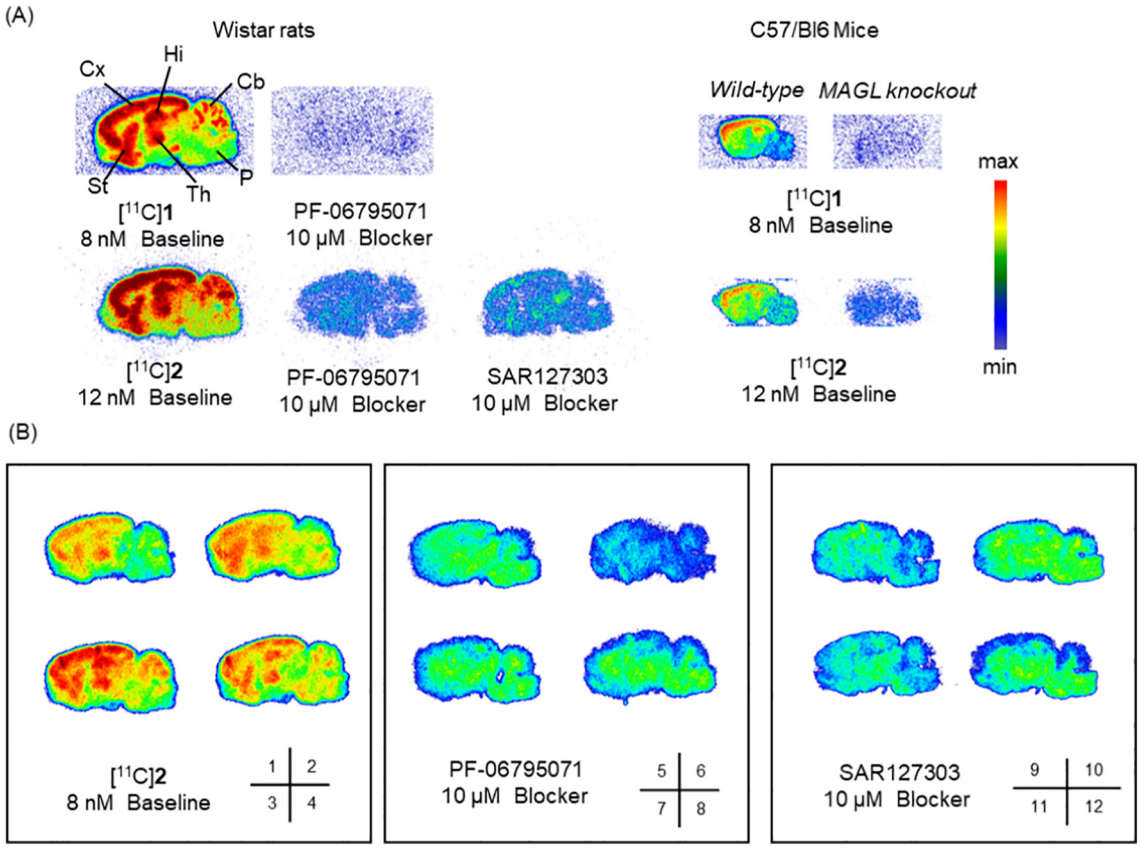

Fig. 2. (A) Representative *in vitro* autoradiograms of [^{11}C]**1** and [^{11}C]**2** obtained from Wistar rat, C57/Bl6 and MAGL knockout mice sagittal brain sections. (B) *In vitro* autoradiography without washing process on Wistar rat brain sections using [^{11}C]**2**. PF06795071 and SAR127303 are covalent MAGL inhibitors. The numbers on the bottom right corner of Fig 2B are corresponding to the entries for semi-quantification in Table 2. Cx, cortex; Hi, hippocampus; Cb, cerebellum; St, striatum; Th, thalamus; P, pons (part of brainstem).

MAGL KO and WT mice were used to evaluate the specificity of [^{11}C]**2** *in vivo*. The whole brain time activity curves (TACs) are illustrated in Fig. 3. [^{11}C]**2** displayed significantly lower brain uptake in MAGL KO mice than those of WT mice indicating specific binding of [^{11}C]**2** *in vivo*. Moreover, [^{11}C]**2** exhibited a slow pharmacokinetic profile in WT mice with a continuously increasing brain uptake until the end of the study. The standardized uptake values (SUVs) of [^{11}C]**2** in various middle time frames in MAGL KO or WT mouse brain from individual scan are summarized in supplementary table S2. To access whether [^{11}C]**2** is recognized as a P-gp substrate in the mouse brain, tariquidar, a P-gp transporter inhibitor, was administrated 45 min before the tracer injection. As illustrated in Fig. 3, the radioactive accumulation of [^{11}C]**2** in the mouse brain significantly increased to 0.92 SUV at 1 min p.i. This result is consistent with its high P-gp efflux ratio in the mouse *in vitro*, confirming that [^{11}C]**2** was recognized as a P-gp substrate in rodents.

Table 2
Semi-quantification of radioactive signals obtained from [^{11}C]**2** in the no-wash *in vitro* autoradiography. The entries are related to the *in vitro* autoradiograms presented in Fig. 2B.

Entry	Type	Area [pixel]	Intensity [PSL]	Density[a] [PSL/pixel]	Average density [PSL/pixel]	%Specific Binding$_{20min}$[b]
1	8 nM [^{11}C]**2**	80,657	55,599	0.69	0.72 ±	–
2		78,211	48,370	0.62	0.09	
3		82,107	64,130	0.78		
4		66,676	53,866	0.81		
5	8 nM [^{11}C]**2**	79,619	32,573	0.41	0.41 ±	44 ± 3
6	+	52,799	18,798	0.36	0.04	
7	10 μM	68,242	29,916	0.44		
8	PF-06809247	75,545	31,746	0.42		
9	8 nM [^{11}C]**2**	60,058	26,683	0.44	0.44 ±	39 ± 13
10	+	72,044	35,007	0.49	0.04	
11	10 μM	65,010	27,214	0.42		
12	SAR127303	76,443	29,999	0.39		

[a] Student's *t*-tests (two-tailed, homoscedastic) were performed for density between different groups (control *vs.* PF-06809247 blocking, $p < 0.001$; control *vs.* SAR127303 blocking, $p < 0.001$).

[b] The '%Specific Binding$_{20min}$' is calculated based on Eq. (2) in the Experimental section.

3.4.2. Radiometabolite analysis

The *in vivo* stability of [^{11}C]**2** was investigated in mouse at 40 min post-injection. UPLC equipped with a radio-detector was applied to analyze the acetonitrile extracts from the brain, plasma and urine samples. Fig. 4 showed their corresponding UPLC chromatograms. In the brain, ≥ 95% of the radioactivity was represented by the intact radioligand ([^{11}C]**2**). Around 33% of the radioactive signals in the plasma sample was [^{11}C]

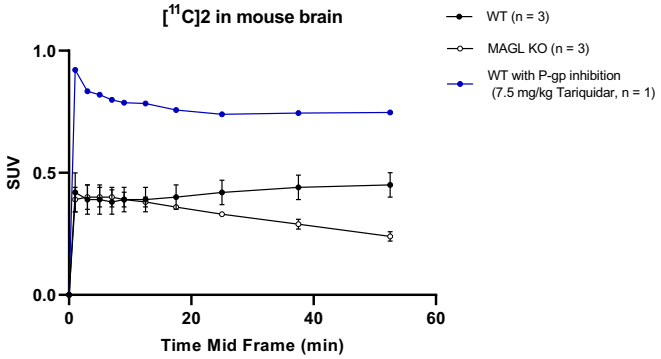

Fig. 3. TACs representing the whole brain accumulation of [^{11}C]**2** in MAGL KO, WT mice under baseline and P-gp blocking conditions.

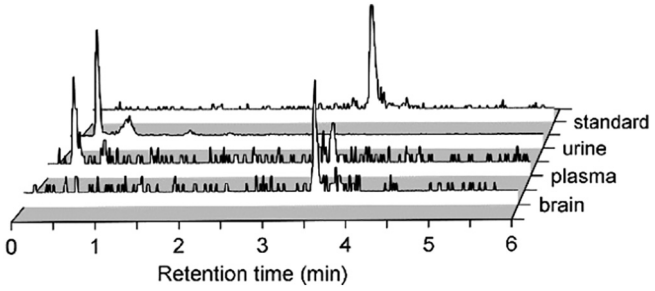

Fig. 4. Radio-UPLC chromatograms of [^{11}C]**2** in radiometabolite analysis at 40 min post-injection.

2, along with a major polar radiometabolite (t_R = 0.332 min). This hydrophilic radiometabolite was also the dominant peak in the urine sample. These results confirmed that the radioactivity accumulated in the mouse brain was contributed primarily by the intact molecular probe without any confounding signals from brain-penetrating radioactive metabolites.

4. Discussion

MAGL has been recognized as a promising therapeutic target in a variety of diseases [28]. Numerous efforts have been made to develop potent and selective PET ligands that can be used to visualize MAGL in the living brain [8]. We have recently discovered a novel class of MAGL inhibitors bearing a morpholine-3-one moiety for the treatment against neuroinflammation and neurodegenerative diseases. To explore their utility as potential reversible MAGL PET ligands, two compounds with high affinity towards MAGL and favorable physiochemical properties *in silico* (CNS MPO score) were selected for radiolabeling and *in vitro*/*in vivo* evaluation.

In vitro studies indicated that compound **2** is slightly superior than **1** in terms of lower IC_{50} values towards mouse and human MAGL (Table 1). Although compound **2** has lower plasma free fraction than compound **1** (11% *vs.* 24% using mouse plasma), the value of 11% is well above the suggested 5% for CNS PET tracers [29]. High P-gp efflux ratios were revealed for both compounds in mice (>6), which made the structures not ideal for imaging MAGL in the mouse brain. However, significantly lower P-gp efflux ratios were obtained from cells transfected with human P-gp (~2.1, see Table 1). Based on these *in vitro* results, we expected that compounds **1** and **2** possess overall favorable properties as potential PET candidates for imaging MAGL in human brains, but moderate-to-low brain uptake in mice. Accordingly, the main objective of our study is to explore whether morpholine-3-one derivatives could serve as a novel class of structures for imaging MAGL by PET.

A modified [^{11}C]CO_2 fixation method was employed for radiolabeling. HHPO and the synthesized azetidine were used as precursors to incorporate carbon-11 into the molecular probes. The isolated radiochemical yields spanned between 1 and 2% over three steps (non-decay corrected), which is comparable to previously reported FAAH radioligand [^{11}C]PF-04457845 (4.5 ± 1.3%, non-decay corrected) using similar radiolabeling approach [30]. As the radiosyntheses gave [^{11}C]**1** and [^{11}C]**2** in sufficient quantities and qualities for all the *in vitro* and *in vivo* evaluations, the radiolabeling condition was not further optimized.

A heterogeneous brain distribution pattern was achieved in *in vitro* autoradiography using either [^{11}C]**1** or [^{11}C]**2** on rat brain sections. These autoradiograms are in accordance with the biological expression of MAGL protein in the rat brain, as well as the results obtained from the irreversible MAGL PET tracer [^{11}C]SAR127303 [27,31]. Moreover, significant reduction of the radioactive signals was seen under blocking conditions and on MAGL KO mouse brain tissues indicating the high specificity and selectivity of the radiotracers *in vitro*. In addition, autoradiographic studies using [^{11}C]**2** on Wistar brain slices without washing procedures was enrolled to mimic the *in vivo* situations as previously described [22]. In agreement with previous results, a heterogeneous distribution reflecting MAGL expression levels in the rat brain was obtained using [^{11}C]**2** without additional washing procedures. Encouraged by these promising *in vitro* results, compound **2** with lower IC_{50} values towards MAGL was selected for further *in vivo* evaluation using MAGL KO and WT mice. A relatively low radioactive accumulation of [^{11}C]**2** in mice brain was observed (*ca.* 0.4 SUV at 1 min p.i.). Pretreatment with 7.5 mg/kg Tariquidar at 45 min before the tracer injection profoundly increased the brain penetration to 0.92 SUV. This result is consistent with the high efflux ratio of compound **2** on cells transfected with mouse P-gp (~6.9, Table 1), and provides strong evidence that low brain uptake of [^{11}C]**2** is associated with P-gp transporters expressing at the mouse blood-brain barrier.

The whole brain uptake of [^{11}C]**2** in MAGL KO mice decreased to 53% of its accumulation level in the WT mouse brains at 60 min after tracer injection. This significant reduction in the level of radioactivity accumulation is in analogue to the *in vivo* results of [^{18}F]T-401 in MAGL KO and WT mice [11], indicating the specific binding of [^{11}C]**2** in the mouse brain. These results suggest that [^{11}C]**2** is a potentially useful MAGL PET tracer *in vivo*. However, the slow kinetic profile of [^{11}C]**2** with the continuously increasing brain uptake up to 60 min p.i. may complicate its quantitative characterization. Radiometabolite analysis revealed that the intact radioligand [^{11}C]**2** is the dominant radioactive form. We therefore concluded that the increasing brain accumulation of [^{11}C]**2** overtime is not related to any brain-penetrating radiometabolites. Of note, slow brain kinetic was commonly expected for MAGL PET tracers with irreversible binding mechanism, such as [^{11}C]SAR127303 and [^{11}C]PF-06809247 [32,33]. Interestingly, it was also recently reported for several reversible MAGL PET tracers including [^{18}F]MAGL-2102 in non-human primates and [^{18}F]MAGL-4-11 in mice [9,10]. A possible explanation for this might be the strong association of these radiotracers with the target *in vivo* [10]. Further studies, which take this issue into account, will need to be undertaken. We are currently working on the *in vitro* assays to characterize the binding interaction between the molecule and the MAGL protein. In the meanwhile, structural optimization on morpholine-3-one scaffold in order to accelerate the clearance from the brain is currently ongoing in our laboratory.

5. Conclusion

Starting from a large morpholine-3-one compound pool, we selected compounds **1** and **2** for carbon-11 labeling due to their high affinity towards the target and favorable physiochemical properties for neuroimaging. Both radiotracers exhibited high specificity and selectivity towards MAGL in *in vitro* autoradiographic studies. *In vivo* specificity of [^{11}C]**2** was demonstrated in PET studies using MAGL KO and WT mice. *Ex vivo* radiometabolite analysis indicated that [^{11}C]**2** displayed high stability in the mouse brain and no entry of radiometabolites from the periphery. In summary, we discovered a novel morpholine-3-one derivative to visualize MAGL in the mouse brain, and [^{11}C]**2** could serve as a lead compound for further structural optimization for non-invasively imaging MAGL by PET *in vivo*.

Acknowledgement

We sincerely thank Marie-Thérèse Miss (Roche Innovation Center Basel) for organizing the MAGL knockout mice, Isabelle Kaufmann (Roche Innovation Center Basel) for the technical assistance, Björn Wagner (Roche Innovation Center Basel) for logD, PAMPA and LIMBA measurements and Carina Cantrill (Roche Innovation Center Basel) for providing the P-gp efflux data. We particularly acknowledge Bruno Mancosu (ETH Zurich) for building up the [^{11}C]CO_2 module for radiolabeling. Yingfang He is grateful for the generous financial support from China Scholarship Council (CSC201706040066).

Declaration of competing interest

The authors declare that they have no known competing financial interests or personal relationships that could have appeared to influence the work reported in this paper.

Appendix A. Supplementary data

Supplementary data to this article can be found online at https://doi.org/10.1016/j.nucmedbio.2022.02.002.

References

[1] Maccarrone M, Bab I, Bíró T, Cabral GA, Dey SK, Di Marzo V, et al. Endocannabinoid signaling at the periphery: 50 years after THC. Trends Pharmacol Sci. 2015;36:277–96. https://doi.org/10.1016/j.tips.2015.02.008.

[2] Maccarrone M. Missing pieces to the endocannabinoid puzzle. Trends Mol Med. 2020;26:263–72. https://doi.org/10.1016/j.molmed.2019.11.002.

[3] Di Marzo V. Targeting the endocannabinoid system: to enhance or reduce? Nat Rev Drug Discov. 2008;7:438–55. https://doi.org/10.1038/nrd2553.

[4] Hillard CJ. Biochemistry and pharmacology of the endocannabinoids arachidonylethanolamide and 2-arachidonylglycerol. Prostaglandins Other Lipid Mediat. 2000;61:3–18. https://doi.org/10.1016/S0090-6980(00)00051-4.

[5] Blankman JL, Simon GM, Cravatt BF. A comprehensive profile of brain enzymes that hydrolyze the endocannabinoid 2-arachidonoylglycerol. Chem Biol. 2007;14:1347–56. https://doi.org/10.1016/j.chembiol.2007.11.006.

[6] Blankman JL, Cravatt BF. Chemical probes of endocannabinoid metabolism. Pharmacol Rev. 2013;65:849–71. https://doi.org/10.1124/pr.112.006387.

[7] Postnov A, Schmidt ME, Pemberton DJ, de Hoon J, van Hecken A, van den Boer M, et al. Fatty acid amide hydrolase inhibition by JNJ-42165279: a multiple-ascending dose and a positron emission tomography study in healthy volunteers. Clin Transl Sci. 2018;11:397–404. https://doi.org/10.1111/cts.12548.

[8] Hou L, Rong J, Haider A, Ogasawara D, Varlow C, Schafroth MA, et al. Positron emission tomography imaging of the endocannabinoid system: opportunities and challenges in radiotracer development. J Med Chem. 2021;64:123–49. https://doi.org/10.1021/acs.jmedchem.0c01459.

[9] Chen Z, Mori W, Deng X, Cheng R, Ogasawara D, Zhang G, et al. Design, synthesis, and evaluation of reversible and irreversible monoacylglycerol lipase positron emission tomography (PET) tracers using a "Tail switching" strategy on a piperazinyl azetidine skeleton. J Med Chem. 2019;62:3336–53. https://doi.org/10.1021/acs.jmedchem.8b01778.

[10] Rong J, Mori W, Xia X, Schafroth MA, Zhao C, Van RS, et al. Novel reversible-binding PET ligands for imaging monoacylglycerol lipase based on the piperazinyl azetidine scaffold. J Med Chem. 2021;64:14283–98. https://doi.org/10.1021/acs.jmedchem.1c00747.

[11] Hattori Y, Aoyama K, Maeda J, Arimura N, Takahashi Y, Sasaki M, et al. Design, synthesis, and evaluation of (4R)-1-{3-[2-(18F)fluoro-4-methylpyridin-3-yl]phenyl}-4-[4-(1,3-thiazol-2-ylcarbonyl)piperazin-1-yl]pyrrolidin-2-one ([18F] T-401) as a novel positron-emission tomography imaging agent for monoacylglycerol lipase. J Med Chem. 2019;62:2362–75. https://doi.org/10.1021/acs.jmedchem.8b01576.

[12] C Bell J Benz L Gobbi U Grether ZK Groebke DJ Hansen, et al. Oxazine monoacylglycerol lipase (MAGL) inhibitors, n.d. https://doi.org/WO2019180185A1.

[13] C Bell J Benz L Gobbi U Grether ZK Groebke B Hornsperger, et al. New heterocyclic compounds as monoacylglycerol lipase inhibitors, n.d. https://doi.org/WO2020035424A1.

[14] L Anselm J Benz U Grether ZK Groebke D Heer B Hornsperger, et al. New heterocyclic compounds as monoacylglycerol lipase inhibitors, n.d. https://doi.org/WO2020035425A1.

[15] Wilson AA, Garcia A, Houle S, Sadovski O, Vasdev N. Synthesis and application of isocyanates radiolabeled with Carbon-11. ChemEur J. 2011;17:259–64. https://doi.org/10.1002/chem.201002345.

[16] Zhang L, Villalobos A, Beck EM, Bocan T, Chappie TA, Chen L, et al. Design and selection parameters to accelerate the discovery of novel central nervous system positron emission tomography (PET) ligands and their application in the development of a novel phosphodiesterase 2A PET ligand. J Med Chem. 2013;56:4568–79. https://doi.org/10.1021/jm400312y.

[17] Gobbi LC, Knust H, Körner M, Honer M, Czech C, Belli S, et al. Identification of three novel radiotracers for imaging aggregated tau in Alzheimer's disease with positron emission tomography. J Med Chem. 2017;60:7350–70. https://doi.org/10.1021/acs.jmedchem.7b00632.

[18] Caruso A, Alvarez-Sánchez R, Hillebrecht A, Poirier A, Schuler F, Lavé T, et al. PK/PD assessment in CNS drug discovery: prediction of CSF concentration in rodents for P-glycoprotein substrates and application to in vivo potency estimation. Biochem Pharmacol. 2013;85:1684–99. https://doi.org/10.1016/j.bcp.2013.02.021.

[19] Schwab D, Fischer H, Tabatabaei A, Poli S, Huwyler J. Comparison of in vitro P-glycoprotein screening assays: recommendations for their use in drug discovery. J Med Chem. 2003;46:1716–25. https://doi.org/10.1021/jm021012t.

[20] Belli S, Assmus F, Wagner B, Honer M, Fischer H, Schuler F, et al. Estimation of drug binding to brain tissue: methodology and in vivo application of a distribution assay in brain polar lipids. Mol Pharm. 2015;12:4529–41. https://doi.org/10.1021/acs.molpharmaceut.5b00717.

[21] Assmus F, Seelig A, Gobbi L, Borroni E, Glaentzlin P, Fischer H. Label-free assay for the assessment of nonspecific binding of positron emission tomography tracer candidates. Eur J Pharm Sci. 2015;79:27–35. https://doi.org/10.1016/j.ejps.2015.08.014.

[22] Patel S, Ndubizu O, Hamill T, Chaudhary A, Burns HD, Hargreaves R, et al. Screening cascade and development of potential positron emission tomography radiotracers for mGluR5: in vitro and in vivo characterization. Mol Imaging Biol. 2005;7:314–23. https://doi.org/10.1007/s11307-005-0005-4.

[23] Kuntner C, Stout D. Quantitative preclinical PET imaging: opportunities and challenges. Front Phys. 2014;2:1–12. https://doi.org/10.3389/fphy.2014.00012.

[24] Joosen MJA, Vester SM, Hamelink J, Klaassen SD, van den Berg RM. Increasing nerve agent treatment efficacy by P-glycoprotein inhibition. Chem Biol Interact. 2016;259:115–21. https://doi.org/10.1016/j.cbi.2016.06.012.

[25] Bankstahl JP, Kuntner C, Abrahim A, Karch R, Stanek J, Wanek T, et al. Tariquidar-induced P-glycoprotein inhibition at the rat blood-brain barrier studied with (R)-11C-verapamil and PET. J Nucl Med. 2008;49:1328–35. https://doi.org/10.2967/jnumed.108.051235.

[26] Mu L, Bieri D, Slavik R, Drandarov K, Müller A, Čermak S, et al. Radiolabeling and in vitro/in vivo evaluation of N-(1-adamantyl)-8-methoxy-4-oxo-1-phenyl-1,4-dihydroquinoline-3-carboxamide as a PET probe for imaging cannabinoid type 2 receptor. J Neurochem. 2013;126:616–24. https://doi.org/10.1111/jnc.12354.

[27] Dinh TP, Carpenter D, Leslie FM, Freund TF, Katona I, Sensi SL, et al. Brain monoglyceride lipase participating in endocannabinoid inactivation. Proc Natl Acad Sci. 2002;99:10819–24. https://doi.org/10.1073/pnas.152334899.

[28] Gil-Ordóñez A, Martín-Fontecha M, Ortega-Gutiérrez S, López-Rodríguez ML. Monoacylglycerol lipase (MAGL) as a promising therapeutic target. Biochem Pharmacol. 2018;157:18–32. https://doi.org/10.1016/j.bcp.2018.07.036.

[29] Honer M, Gobbi L, Martarello L, Comley RA. Radioligand development for molecular imaging of the central nervous system with positron emission tomography. Drug Discov Today. 2014;19:1936–44. https://doi.org/10.1016/j.drudis.2014.08.012.

[30] Hicks JW, Parkes J, Sadovski O, Tong J, Houle S, Vasdev N, et al. Synthesis and preclinical evaluation of [11C-carbonyl]PF-04457845 for neuroimaging of fatty acid amide hydrolase. Nucl Med Biol. 2013;40:740–6. https://doi.org/10.1016/j.nucmedbio.2013.04.008.

[31] Yamasaki T, Mori W, Zhang Y, Hatori A, Fujinaga M, Wakizaka H, et al. First demonstration of in vivo mapping for regional brain monoacylglycerol lipase using PET with [11C]SAR127303. Neuroimage. 2018;176:313–20. https://doi.org/10.1016/j.neuroimage.2018.05.015.

[32] Wang C, Placzek MS, Van De Bittner GC, Schroeder FA, Hooker JM. A novel radiotracer for imaging monoacylglycerol lipase in the brain using positron emission tomography. ACS Chem Nerosci. 2016;7:484–9. https://doi.org/10.1021/acschemneuro.5b00293.

[33] Zhang L, Butler CR, Maresca KP, Takano A, Nag S, Jia Z, et al. Identification and development of an irreversible monoacylglycerol lipase (MAGL) positron emission tomography (PET) radioligand with high specificity. J Med Chem. 2019;62:8532–43. https://doi.org/10.1021/acs.jmedchem.9b00847.